doi:10.1093/brain/awz162 BRAIN 2019: 142; 2483–2491 | 2483

BRAIN
A JOURNAL OF NEUROLOGY

White matter hyperintensities: relationship to amyloid and tau burden

Jonathan Graff-Radford,[1] Eider M. Arenaza-Urquijo,[2] David S. Knopman,[1] Christopher G. Schwarz,[2] Robert D. Brown, Jr,[1] Alejandro A. Rabinstein,[1] Jeffrey L. Gunter,[2] Matthew L. Senjem,[2] Scott A. Przybelski,[3] Timothy Lesnick,[3] Chadwick Ward,[2] Michelle M. Mielke,[1,3] Val J. Lowe,[2] Ronald C. Petersen,[1] Walter K. Kremers,[3] Kejal Kantarci,[2] Clifford R. Jack Jr[2] and Prashanthi Vemuri[2]

Although white matter hyperintensities have traditionally been viewed as a marker of vascular disease, recent pathology studies have found an association between white matter hyperintensities and Alzheimer's disease pathologies. The objectives of this study were to investigate the topographic patterns of white matter hyperintensities associated with Alzheimer's disease biomarkers measured using PET. From the population-based Mayo Clinic Study of Aging, 434 participants without dementia (55% male) with FLAIR and gradient recall echo MRI, tau-PET (AV-1451) and amyloid-PET scans were identified. A subset had cerebral microbleeds detected on T_2* gradient recall echo scans. White matter hyperintensities were semi-automatically segmented using FLAIR MRI in participant space and normalized to a custom template. We used statistical parametric mapping 12-based, voxel-wise, multiple-regression analyses to detect white matter hyperintense regions associated with Alzheimer's biomarkers (global amyloid from amyloid-PET and meta-regions of interest tau uptake from tau-PET) after adjusting for age, sex and hypertension. For amyloid associations, we additionally adjusted for tau and vice versa. Topographic patterns of amyloid-associated white matter hyperintensities included periventricular white matter hyperintensities (frontal and parietal lobes). White matter hyperintense volumes in the detected topographic pattern correlated strongly with lobar cerebral microbleeds ($P < 0.001$, age and sex adjusted Cohen's $d = 0.703$). In contrast, there were no white matter hyperintense regions significantly associated with increased tau burden using voxel-based analysis or region-specific analysis. Among non-demented elderly, amyloid load correlated with a topographic pattern of white matter hyperintensities. Further, the amyloid-associated, white matter hyperintense regions strongly correlated with lobar cerebral microbleeds suggesting that cerebral amyloid angiopathy contributes to the relationship between amyloid and white matter hyperintensities. The study did not support an association between increased tau burden and white matter hyperintense burden.

1 Department of Neurology, Mayo Clinic, Rochester, Minnesota, USA
2 Department of Radiology, Mayo Clinic, Rochester, Minnesota, USA
3 Department of Health Sciences Research, Mayo Clinic, Rochester, Minnesota, USA

Correspondence to: Dr Jonathan Graff-Radford
Assistant Professor of Neurology, Mayo Clinic College of Medicine
200 1st Street SW, Rochester, MN, 55905, USA
E-mail: Graff-Radford.Jonathan@mayo.edu

Keywords: white matter hyperintensities; cerebral microbleeds; cerebral amyloid angiopathy; tau burden

Abbreviations: CAA = cerebral amyloid angiopathy; CMB = cerebral microbleed; SUVR = standardized uptake value ratio; WMH = white matter hyperintensities

Received January 16, 2019. Revised April 2, 2019. Accepted April 18, 2019. Advance Access publication June 14, 2019

Introduction

White matter hyperintensities (WMH) are commonly detected on FLAIR MRI and increase with age. WMH are considered a manifestation of cerebral small vessel disease (Pantoni, 2010) and coincide with other imaging markers of cerebral small vessel disease. The most consistent risk factors for WMH development are age and hypertension (de Leeuw *et al.*, 2002; Gottesman *et al.*, 2010; Verhaaren *et al.*, 2013). Cerebral amyloid angiopathy (CAA), another cerebral small vessel disease, has also been shown to be a risk factor for WMH. There is increased WMH burden among subjects with CAA compared to subjects without CAA (Holland *et al.*, 2008), and amyloid burden and WMH in CAA are strongly correlated (Gurol *et al.*, 2013).

Recent literature has focused on understanding the relationships between WMH and Alzheimer's disease pathologies. In autosomal dominant Alzheimer's disease, WMH burden was found to be greater than in controls and associated with cerebral microbleeds (CMBs) (Lee *et al.*, 2018). Among amyloid-positive individuals, those with a diagnosis of Alzheimer's disease dementia have greater WMH than those who are cognitively unimpaired (Provenzano *et al.*, 2013). Imaging pathological studies in Alzheimer's disease dementia participants have also shown a relationship between tau burden and WMH (Erten-Lyons *et al.*, 2013), particularly in the parietal lobes (McAleese *et al.*, 2015). These studies suggest that degenerative pathologies contribute to WMH, in addition to cerebrovascular disease. Whether Alzheimer's disease pathologies contribute significantly to WMH in the general population remains unclear. Using the Mayo Clinic Study of Aging, we investigated the relationship between Alzheimer's disease pathologies and WMH *in vivo* in a population-based setting. Given the availability of amyloid-PET and tau-PET for detection of Alzheimer's disease pathologies, our study objective was to determine the anatomical associations between WMH and Alzheimer's disease pathologies in the general population.

Materials and methods

Study participants

Participants, aged 50 to 89, were enrolled in the Mayo Clinic Study of Aging (MCSA), a population-based study of Olmsted County, Minnesota residents. The Rochester Epidemiology Project (REP) medical records linkage system was used to enumerate the Olmsted County population (St Sauver *et al.*, 2012). Randomly selected participants from Olmsted County were invited to participate in the study. This study included 434 non-demented participants with FLAIR-MRI, tau-PET (AV-1451) and Pittsburgh compound B (PiB)-PET (amyloid) scans to assess the relationship between FLAIR WMH and Alzheimer's disease pathologies. Using the medical records linkage system, a nurse abstracted the history of hypertension (St Sauver *et al.*, 2011).

Cognitive assessment

Participants underwent a neuropsychological battery encompassing four cognitive domains: (i) memory; (ii) attention-executive function; (iii) language; and (iv) visuospatial skills (Roberts *et al.*, 2008). In addition to the neuropsychological testing, participants were evaluated by a study coordinator and physician. A past medical history review and interview with a study partner and participant was performed by the study coordinator, and a physician completed the mental status and neurological examinations. Subsequently, at a consensus conference with the examining physician, study coordinator, and neuropsychologist, participants were classified cognitively as has been described previously (Roberts *et al.*, 2008). Participants were assigned a diagnosis of cognitively unimpaired [not mild cognitive impairment (MCI) or dementia] using previously published criteria (Petersen, 2004; McKhann *et al.*, 2011) or MCI (Petersen *et al.*, 2019).

Standard protocol approvals, registrations and patient consents

These studies were approved by the Mayo Clinic and Olmsted Medical Center Institutional Review Boards. Written informed consent was obtained from all participants.

FLAIR MRI assessment of white matter hyperintensities

All MRI images were acquired on 3 T MRI scanners (GE Healthcare). We used both the T_1-weighted MPRAGE image and FLAIR image of each individual for the WMH segmentation. FLAIR MRI scans with repetition time = 11 000 ms, echo time = 147 ms, inversion time = 2250 ms, 256 × 192 matrix, 24-cm field of view and 3-mm slice thickness were carried out to quantify WMH volume (Kantarci *et al.*, 2013*b*). Briefly, we first identified possible WMH voxels through clustering via connected components using the FLAIR images. We then used SPM5 segmentations from T_1-weighted image aligned to the FLAIR images and corresponding brain masks to remove non-brain tissue and voxels that had a high likelihood of being grey matter and not likely WMH. Additional clusters were excluded if they occurred external to areas categorized as white matter, made up of a single isolated voxel, or had no supra-threshold FLAIR voxels after blurring. The WMH masks identified through this process were then manually edited by trained image analysts to fix incorrect WMH classifications to ensure consistent WMH segmentation across participants. Voxels associated with infarcts were removed and not considered as part of the WMH measurement.

We then normalized the edited WMH masks to Mayo Clinic Adult Lifespan Template (MCALT) (Schwarz *et al.*, 2017) space (https://www.nitrc.org/projects/mcalt) by applying the rigid registration between the FLAIR scan and the corresponding T_1-weighted MRI, then applying normalization parameters for the T_1-weighted MRI, previously computed with statistical parametric mapping 12, and resampling using nearest neighbour.

These normalized segmentation masks were smoothed by a 6 mm full-width at half-maximum (FWHM) Gaussian kernel prior to performing voxel-based analyses.

MRI examination of cerebral microbleeds

All participants also underwent T_2* gradient recall echo (repetition time/echo time = 200/20 ms; flip angle = 12°; in-plane matrix = 256 × 224; phase field of view = 1.00; slice thickness = 3.3 mm; acquisition time was 5 min). CMBs were graded on T_2* sequences and defined based on current consensus criteria (Greenberg *et al.*, 2009; Kantarci *et al.*, 2013*a*). All possible CMBs were marked by trained image analysts and subsequently confirmed by a vascular neurologist or radiologist experienced in reading the T_2* gradient recall echo blinded to the participants' clinical information (Graff-Radford *et al.*, 2019). We only included strictly lobar CMBs, which may be a marker of CAA.

Amyloid and tau PET markers

Amyloid-PET imaging was carried out with ^{11}C-PiB. Tau PET was carried out with AV-1451, synthesized on site with precursor supplied by Avid Radiopharmaceuticals (Schwarz *et al.*, 2016). Late-uptake amyloid-PET images were acquired 40–60 min and tau-PET 80–100 min after injection. CT was obtained for attenuation correction.

Amyloid-PET and tau-PET were analysed with our in-house fully automated image-processing pipeline, where image voxel values were extracted from automatically labelled regions of interest propagated from the MCALT template (Senjem *et al.*, 2005). Amyloid-PET and tau-PET standardized uptake value ratio (SUVR) values were formed by normalizing target regions of interest to the cerebellar Crus grey matter (Jack *et al.*, 2017*a*).

An amyloid-PET SUVR was formed from previously published regions of interest (Jack *et al.*, 2017*a*) normalized to the cerebellar Crus grey median. A tau-PET meta-region of interest was formed from a voxel number-weighted average of the median uptake in previously published regions of interest (Jack *et al.*, 2017*a*) normalized to the cerebellar Crus grey median. The tau-PET meta-region of interest was composed of the entorhinal, amygdala, parahippocampal, fusiform, inferior temporal, and middle temporal regions of interest. This meta-region of interest was selected as it has previously been used in cognitively unimpaired individuals and increases with age as expected (Jack *et al.*, 2017*b*).

The participants' MRI scans were used for the quantification of the PET images. PET data were not corrected for partial volume.

Statistical analysis

Demographic and clinical characteristics of the participants were summarized using means and standard deviations for continuous variables and counts and percentages for categorical variables. We also provided the demographic characteristics and imaging biomarkers categorized by clinical status in Supplementary Table 1. The distributions of the continuous variables were examined for approximate symmetry and normality using plots; PiB SUVR was subsequently log-transformed for statistical tests to reduce a positive skew. There were two analyses as part of this study: (i) SPM analyses to investigate the associations between voxel-level WMH and Alzheimer's disease biomarkers; and (ii) associations between the WMH volumes in the detected WMH regions with lobar CMBs.

Associations between white matter hyperintensity maps, global amyloid and tau

We conducted a voxel-wise multiple regression analysis in SPM 12 (Ashburner, 2009) to detect spatial associations between Alzheimer's disease biomarkers (global amyloid from amyloid-PET and meta-region of interest tau uptake from tau-PET) and WMH maps. Smoothed WMH maps (dependent variable), PiB ratio, tau meta-region of interest, age, sex and history of hypertension (predictor variables) were entered into the model. A study-specific, white matter mask, thresholded to include voxels with a white matter probability >0.25, was used as explicit mask for the analysis. We tested the independent effects of total amyloid and tau meta-region of interest on WMH (i.e. for amyloid associations, results were adjusted for tau and vice versa). Resulting t-maps from the voxel-wise analyses were thresholded and binarized to create two whole-brain binary masks that reflected the spatial associations between Alzheimer's disease biomarkers and WMH with greater sensitivity or specificity. Our main analyses consisted of WMH regions detected with voxel-level threshold of false discovery rate (FDR)-corrected $P < 0.05$. We label this mask as a sensitivity mask (higher sensitivity detection). In addition, we also applied a more stringent FDR-corrected $P < 0.001$ for the specific mask in order to identify those regions with greater spatial specificity. In both cases, we additionally applied a threshold of FWE-corrected $P < 0.05$ at cluster level. The total WMH burden (volume cm^3) within these masks was used in a second step to assess associations with CMBs.

To assess and provide a visual reference of the sensitivity/specificity of the maps created from the voxel-wise analyses, we generated a frequency map to visualize the proportion of study participants with WMH in a specific spatial location. Normalized WMH maps were added, averaged and multiplied by 100.

Associations between specific and sensitive masks and lobar microbleeds

To determine whether the amyloid load-related WMH masks were driven in part by CAA, we performed an exploratory analysis to test the association between WMH volume in the masks and CMBs. We categorized individuals based on the presence of strictly lobar CMBs = 0 and $\geqslant 2$ and compared the WMH volumes in the specific and sensitive masks between these two categories. As two or more strictly lobar CMBs are a diagnostic biomarker of CAA (Greenberg and Charidimou, 2018), we also estimated the effect sizes of associations between lobar CMB $\geqslant 2$ versus 0 CMBs and the WMH volumes in these masks.

Data availability

Data from the Mayo Clinic Study of Aging, including data from this study, are available upon request.

Table 1 Characteristics with the mean (SD) listed for the continuous variables and count (%) for the categorical variables

	All $n = 424$
Demographics	
Males, *n* (%)	233 (55)
Age, years	75.0 (8.4)
ε4 carrier, *n* (%)	120 (28%)
Education, years	14.8 (2.6)
Hypertension, *n* (%)	259 (61)
Cognitively impaired (%)	33 (8)
Global cognitive z-score	0.15 (1.07)
Imaging	
Amyloid-PET SUVR	1.57 (0.41)
Tau-PET SUVR	1.21 (0.10)

Results

Table 1 summarizes the characteristics of the participants. Three hundred and ninety-one participants were cognitively unimpaired and 33 participants had MCI.

Association of amyloid-PET with white matter hyperintensities

After adjusting for age, sex, hypertension and tau SUVR, the topographic amyloid-associated WMH patterns after both voxel and cluster level corrections primarily included periventricular WMH (frontal and parietal lobes). Table 2 shows the anatomical labels, peak coordinates, cluster sizes, and statistics of the voxel-wise multiple regression.

Masks with lenient (greater detection sensitivity) and strict thresholds (greater detection specificity) are shown in the Fig. 1. The visual comparison between the three maps strikingly shows that the specificity mask captures the areas of higher WMH frequency in the study population. The mask with greater sensitivity covered most of the high WMH frequency regions that are seen across the study population with the largest cluster in the posterior cingulum bundle. The mask with greater specificity was sparse, with the largest clusters in the frontal and parietal lobes.

Association of tau-PET with white matter hyperintensities

After adjusting for age, sex, hypertension and amyloid load, there were no WMH regions significantly associated with increased global tau burden. We also investigated regional associations using a lobar atlas in the MCALT (Schwarz *et al.*, 2017) space. We did not find any significant positive associations between WMH burden within each lobe with tau-PET SUVR extracted in the same region (Fig. 2). Without adjusting for amyloid, we still found no associations between WMH and tau [r = 0.0036 ($P > 0.1$)].

We tested for tau × sex and amyloid × sex interactions on WMH burden. There were no significant interaction effects, suggesting that the results did not differ by sex.

White matter hyperintensity masks and cerebral microbleeds

Table 3 reports the characteristics and associations with the WMH masks for those with ⩾2 lobar CMBs compared to those with 0 lobar CMBs. A box plot of WMH in the sensitive and specific masks as a function of ⩾2 lobar CMBs is shown in Fig. 3. Seventeen participants had ⩾2 strictly lobar CMBs. Both the sensitive ($P < 0.001$, age and sex-adjusted Cohen's $d = 0.703$) and specific ($P < 0.001$, age and sex-adjusted Cohen's $d = 0.68$) WMH maps were strongly associated with ⩾2 lobar CMBs after adjusting for age.

Discussion

In the study of non-demented individuals, we found that amyloid burden measured by PET was associated with a topographic pattern of WMH. These amyloid-related WMH regions were associated with lobar CMBs suggesting that regional changes correlate with CAA. We found no evidence to support an association between tau burden and WMH burden.

Prior studies have shown that WMH develop in areas of low white matter perfusion, and areas with lower cerebral blood flow adjacent to WMH are associated with future WMH development (Promjunyakul *et al.*, 2015). In mouse models of parenchymal amyloid deposition and CAA, cerebral blood flow is unchanged when amyloid is only present in the parenchyma but is reduced with CAA (Maier *et al.*, 2014). Among individuals with at least one lobar CMB, the parietal lobe had the largest decrease in blood flow compared to those without lobar CMBs, although the frontal cortex, precuneus, and anterior cingulate also show decreased cerebral blood flow relative to controls (Gregg *et al.*, 2015). It is possible that regions with reduced cerebral blood flow in individuals with lobar CMBs, a marker of CAA, are most susceptible to WMH.

Regional white matter hyperintensity associations with amyloid deposition and mechanistic basis

A prior study demonstrated that WMH burden was associated with amyloid burden among CAA participants but not those with a diagnosis of Alzheimer's disease dementia or those who were cognitively unimpaired (Gurol *et al.*, 2013). Therefore, we sought to determine whether lobar CMBs (a surrogate of CAA pathology) are associated with a WMH mask related to amyloid burden. After

Table 2 Anatomical labels, cluster size (mm^3), voxel and cluster corrected *P*-values, t-values and peak voxel coordinates of the areas of positive association between PiB ratio and smoothed WMH probability maps, adjusted by age, sex, hypertension, and tau meta-region of interest

	Cluster size, mm^3	Cluster $P_{FWE\text{-}corr}$	Peak $P_{FWE\text{-}corr}$	T-value	Coordinates		
					x	*y*	*z*
Sensitivity mask							
L Parietal (posterior cingulum)	67281	<0.001	<0.001	6.05	−20	−57	36
		<0.001	<0.001	5.46	−21	−45	44
		0.001	<0.001	5.32	−27	−56	−3
R Parietal (posterior cingulum)	68097	0.001	<0.001	5.23	22	−66	0
		0.002	<0.001	5.17	22	−58	30
		0.002	<0.001	5.13	27	0	40
Specific mask							
L Parietal (posterior cingulum)	2720	<0.001	<0.001	6.05	−20	−57	36
			<0.001	5.46	−21	−45	44
L occipital (inf. longitudinal fasc.)	246	0.034	<0.001	5.32	−27	−56	−3
L frontal (sup. corona radiata)	5781	<0.001	<0.001	5.28	−24	14	33
			<0.001	5.05	−26	−6	33
			<0.001	4.98	−22	24	24
R occipital (inf. longitudinal fasc.)	500	0.012	<0.001	5.23	22	−66	0
R occipital (inf. fronto-occipital fasc.)	776	0.005	<0.001	5.17	22	−58	30
			<0.001	4.72	21	−64	24
			0.001	4.13	14	−57	28
R frontal (sup. longitudinal fasc.)	1104	0.002	<0.001	5.13	27	0	40
			<0.001	5	21	−6	40
R parietal (inf longitudinal fasc.)	908	0.003	<0.001	4.84	21	−44	39
			<0.001	4.76	16	−51	42
L occipital (inf longitudinal fasc.)	213	0.04	<0.001	4.83	−21	−70	−2
R frontal (genu of corpus callosum)	645	0.007	<0.001	4.75	14	33	9
R frontal (anterior corona radiata)	341	0.022	0.001	4.32	21	21	24
			0.001	4.25	12	24	18

Coordinates are given in MCAL template space. fasc. = fasciculus; inf. = inferior; L = left; R = right; sup = superior.

creating masks of these WMH patterns, we investigated whether these regions are associated with CMB burden. The WMH masks associated with amyloid burden are similar in appearance to the overall frequency map of WMH (Fig. 1C); therefore, the pattern detected should not be viewed as specific to amyloid. Although we had a limited number of individuals with multiple lobar CMBs, we found that these WMH masks were associated with lobar CMBs suggesting that CAA contributes to the relationship between amyloid and WMH. We also found support for this hypothesis when we found that the association between WMH masks and amyloid was slightly attenuated when lobar CMBs were taken into account. DIAN investigators also demonstrated that autosomal dominant mutation carriers with Alzheimer's disease had greater WMH burden than non-carriers and that ~20% of the relationship between mutation status and WMH was mediated by CMBs. This finding suggests that CAA contributes to the development of WMH but does not fully explain the relationship (Lee *et al.*, 2018). Prior studies have shown that patients with CAA have greater WMH burden than controls (Holland *et al.*, 2008). Compared to individuals with an intracerebral haemorrhage due to hypertension and WMH in deep regions, those with CAA have more subcortical WMH (Charidimou *et al.*, 2016). Therefore, vascular amyloid appears to be an important contributor to the development of WMH. Recently we have shown that lobar but not deep CMBs are associated with amyloid burden in the general population (Graff-Radford *et al.*, 2019). The development of these white matter masks associated with amyloid burden and lobar CMBs reflects, in part, a contribution of CAA to WMH burden and will be helpful for future studies investigating small vessel disease associated with underlying CAA.

Lack of association of white matter hyperintensities with tau burden

We did not detect an association between tau burden and WMH in either the voxel-level analyses or region-level analyses. In the voxel-level analyses, we used a tau-PET measure focused on the temporal lobe, which captures Alzheimer's disease-specific tau burden, and did not find any effect of global tau on regional WMH. To confirm these results, we also repeated the analyses using regional data to test whether there were associations of local tau

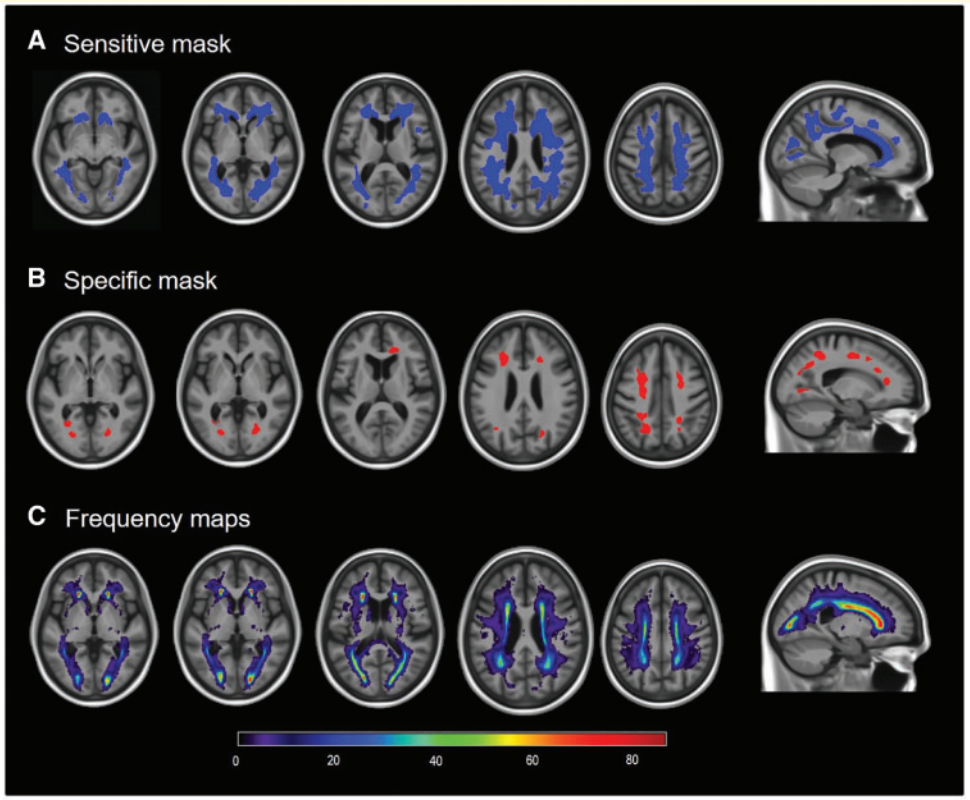

Figure 1 Results of the voxel-wise multiple regression analyses and frequency maps. (**A** and **B**) Areas of positive associations between amyloid-PET SUVR and WMHs adjusted by age, sex, hypertension and tau meta-region of interest. (**A**) The sensitive mask, and (**B**) the specific mask. (**C**) The frequency of WMHs in the study sample, ranging from very infrequent (dark blue colours) to very frequent (green to red colours).

Table 3 Characteristics with the mean (SD) listed for the continuous variables and count (%) for the categorical variables

	Lobar = 0, *n* = 338	Lobar ⩾ 2, *n* = 17	*P*-value	Cohen's *d*	Adjusted Cohen's *d*
Demographics[a]					
Males, *n* (%)	177 (52)	13 (76)	0.05	0.484	
Age, years	73.9 (8.0)	81.3 (7.5)	<0.001	0.929	
Imaging[b]					
WMH sensitive mask, cm^3	7.5 (10.2)	22.6 (18.5)	0.004	1.127	0.703
WMH specific mask, cm^3	0.6 (1.2)	2.5 (2.8)	0.005	1.099	0.68

[a]*P*-values for differences between groups come from a t-test for the continuous variables or a chi-squared test for the categorical variables.
[b]Cohen's *d* and *P*-values for differences between groups come from an ANCOVA adjusted for age and sex with the ranks for the imaging biomarkers.

with local development of WMH and found no evidence to support the hypothesis. This is in contrast to pathological studies, which have shown a relationship between parietal tau and WMH burden (McAleese *et al.*, 2015). Because amyloid is a significant driver of tau deposition and amyloid and WMH are related, we had to additionally adjust for amyloid when investigating associations between WMH and tau. Even without adjusting for amyloid, we found no associations between WMH and tau.

Several possible reasons exist for the lack of associations between WMH and tau in our study. Our population consisted of non-demented individuals. These individuals tend to have a low overall tau burden (Jack *et al.*, 2017*a*) compared to the pathology studies that included individuals with Alzheimer's disease dementia at autopsy and likely represented the severe end of the tauopathy spectrum. Different results may have been found if the same evaluation were conducted in individuals with more advanced neurodegenerative disease and established cognitive impairment. Finally, the detection sensitivity of AV-1451 may be insufficient to see early tau that is captured at autopsy (Lowe *et al.*, 2016). Overall, it is important to

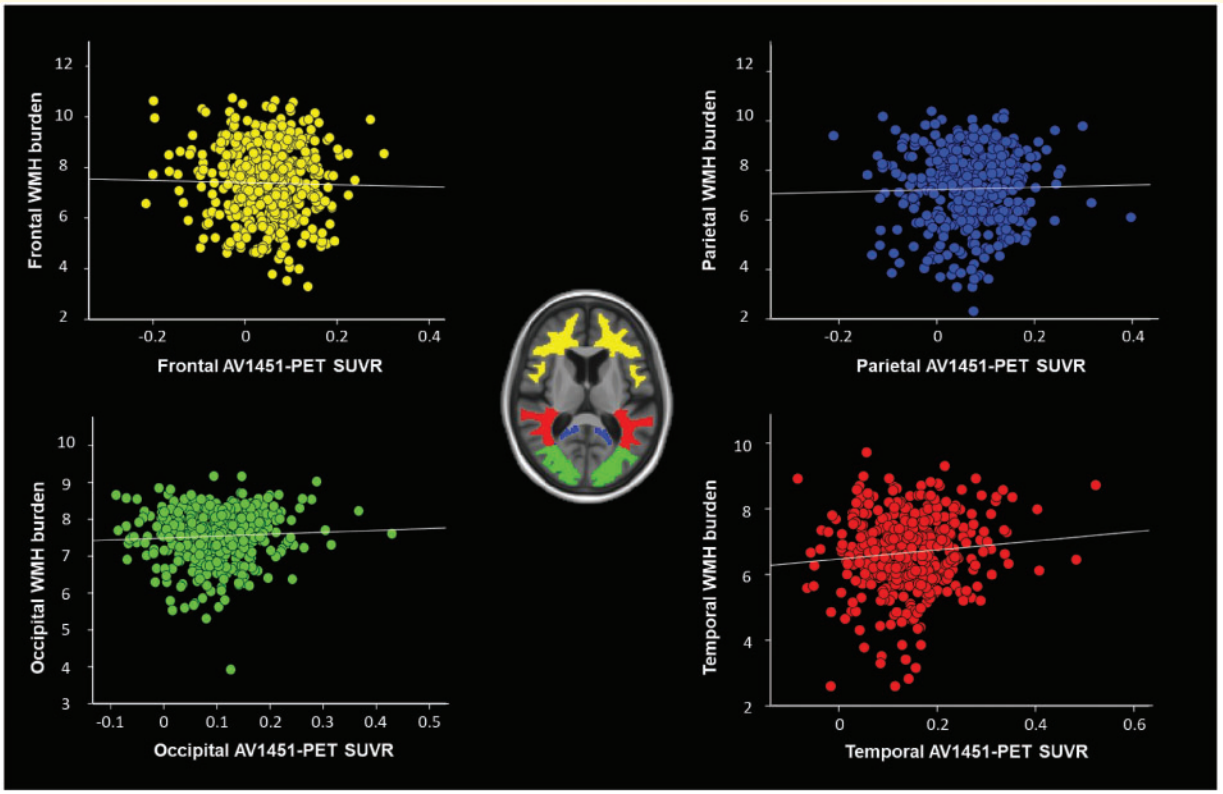

Figure 2 Log (WMH) plotted against log (tau-PET SUVR) in different lobes. There were no significant associations between the two variables after accounting for age, sex, amyloid load and hypertension.

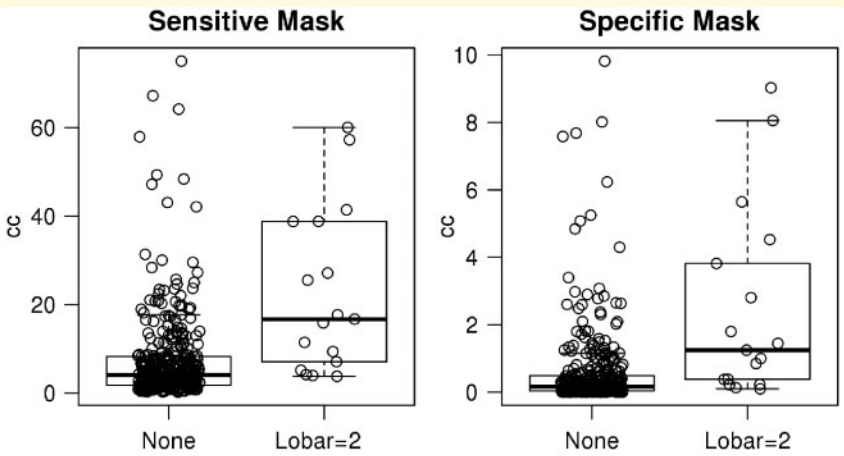

Figure 3 Box plot of WMH in the sensitive and specific masks as a function of two or more lobar CMBs. *y*-axis is volume of WMH.

note that the results we found in non-demented individuals cannot be generalized to patients with dementia.

This study has some limitations. Because our population was restricted to non-demented individuals, those with the highest tau burden (Alzheimer's disease dementia) were excluded. Individuals with both high tau levels and high WMH are more likely to have dementia. Future studies will investigate the relationship between tau burden and WMH in demented individuals, which would better correspond with the work done in most neuropathology studies.

Among non-demented elderly individuals, amyloid load correlated with a topographic pattern of WMH. The topographic pattern of WMH correlated with CMB burden, which suggests that these masks reflect the contribution of CAA to WMH. No relationship was found between tau burden and WMH suggesting that tau does not play

a significant role in the pathogenesis of WMH in non-demented individuals.

Acknowledgements

We would like to thank AVID Radiopharmaceuticals, Inc., for their support in supplying AV-1451 precursor, chemistry production advice and oversight, and FDA regulatory cross-filing permission and documentation needed for this work.

Funding

This work was funded by the National Institute on Aging R37 AG011378 (C.R.J.), K76 AG057015 (J.G-R.), R01 AG041851 (C.R.J. and D.S.K.), U01 AG006786 (R.C.P.), R01 AG034676 (Dr Rocca, PI of the REP study), and R01 AG56366 (P.V.); the National Institute of Neurologic Disorders and Stroke R01 NS097495 (P.V.), and a grant from the GHR Foundation. The sponsors had no role in the development of this study.

Competing interests

The authors report no competing interests.

Supplementary material

Supplementary material is available at *Brain* online.

References

Ashburner J. Computational anatomy with the SPM software. Magn Reson Imaging 2009; 27: 1163–74.

Charidimou A, Boulouis G, Haley K, Auriel E, van Etten ES, Fotiadis P, et al. White matter hyperintensity patterns in cerebral amyloid angiopathy and hypertensive arteriopathy. Neurology 2016; 86: 505–11.

de Leeuw FE, de Groot JC, Oudkerk M, Witteman JC, Hofman A, van Gijn J, et al. Hypertension and cerebral white matter lesions in a prospective cohort study. Brain 2002; 125: 765–72.

Erten-Lyons D, Woltjer R, Kaye J, Mattek N, Dodge HH, Green S, et al. Neuropathologic basis of white matter hyperintensity accumulation with advanced age. Neurology 2013; 81: 977–83.

Gottesman RF, Coresh J, Catellier DJ, Sharrett AR, Rose KM, Coker LH, et al. Blood pressure and white-matter disease progression in a biethnic cohort: atherosclerosis risk in communities (ARIC) study. Stroke 2010; 41: 3–8.

Graff-Radford J, Botha H, Rabinstein AA, Gunter JL, Przybelski SA, Lesnick T, et al. Cerebral microbleeds: prevalence and relationship to amyloid burden. Neurology 2019; 92: e253–62.

Greenberg SM, Charidimou A. Diagnosis of cerebral amyloid angiopathy: evolution of the boston criteria. Stroke 2018; 49: 491–7.

Greenberg SM, Vernooij MW, Cordonnier C, Viswanathan A, Al-Shahi Salman R, Warach S, et al. Cerebral microbleeds: a guide to detection and interpretation. Lancet Neurol 2009; 8: 165–74.

Gregg NM, Kim AE, Gurol ME, Lopez OL, Aizenstein HJ, Price JC, et al. incidental cerebral microbleeds and cerebral blood flow in elderly individuals. JAMA Neurol 2015; 72: 1021–8.

Gurol ME, Viswanathan A, Gidicsin C, Hedden T, Martinez-Ramirez S, Dumas A, et al. Cerebral amyloid angiopathy burden associated with leukoaraiosis: a positron emission tomography/magnetic resonance imaging study. Ann Neurol 2013; 73: 529–36.

Holland CM, Smith EE, Csapo I, Gurol ME, Brylka DA, Killiany RJ, et al. Spatial distribution of white-matter hyperintensities in Alzheimer disease, cerebral amyloid angiopathy, and healthy aging. Stroke 2008; 39: 1127–33.

Jack CR Jr, Wiste HJ, Weigand SD, Therneau TM, Lowe VJ, Knopman DS, et al. Defining imaging biomarker cut points for brain aging and Alzheimer's disease. Alzheimers Dement 2017a; 13: 205–16.

Jack CR, Wiste HJ, Weigand SD, Therneau TM, Knopman DS, Lowe V, et al. Age and sex specific prevalences of cerebral β-amyloidosis, tauopathy and neurodegeneration among clinically normal individuals aged 50–95 years: a cross-sectional study. Lancet Neurol 2017b; 16: 435–44.

Kantarci K, Gunter JL, Tosakulwong N, Weigand SD, Senjem MS, Petersen RC, et al. Focal hemosiderin deposits and beta-amyloid load in the ADNI cohort. Alzheimers Dement 2013a; 9: S116–23.

Kantarci K, Weigand SD, Przybelski SA, Preboske GM, Pankratz VS, Vemuri P, et al. MRI and MRS predictors of mild cognitive impairment in a population-based sample. Neurology 2013b; 81: 126–33.

Lee S, Zimmerman ME, Narkhede A, Nasrabady SE, Tosto G, Meier IB, et al. White matter hyperintensities and the mediating role of cerebral amyloid angiopathy in dominantly-inherited Alzheimer's disease. PLoS One 2018; 13: e0195838.

Lowe VJ, Curran G, Fang P, Liesinger AM, Josephs KA, Parisi JE, et al. An autoradiographic evaluation of AV-1451 Tau PET in dementia. Acta Neuropathol Commun 2016; 4: 58.

Maier FC, Wehrl HF, Schmid AM, Mannheim JG, Wiehr S, Lerdkrai C, et al. Longitudinal PET-MRI reveals β-amyloid deposition and rCBF dynamics and connects vascular amyloidosis to quantitative loss of perfusion. Nat Med 2014; 20: 1485.

McAleese KE, Firbank M, Dey M, Colloby SJ, Walker L, Johnson M, et al. Cortical tau load is associated with white matter hyperintensities. Acta Neuropathol Commun 2015; 3: 60.

McKhann GM, Knopman DS, Chertkow H, Hyman BT, Jack CR, Kawas CH, et al. The diagnosis of dementia due to Alzheimer's disease: recommendations from the National Institute on Aging-Alzheimer's Association workgroups on diagnostic guidelines for Alzheimer's disease. Alzheimers Dement 2011; 7: 263–9.

Pantoni L. Cerebral small vessel disease: from pathogenesis and clinical characteristics to therapeutic challenges. Lancet Neurol 2010; 9: 689–701.

Petersen RC. Mild cognitive impairment as a diagnostic entity. J Intern Med 2004; 256: 183–94.

Petersen RC, Lundt ES, Therneau TM, Weigand SD, Knopman DS, Mielke MM, et al. Predicting progression to mild cognitive impairment. Ann Neurol 2019; 85: 155–60.

Promjunyakul N, Lahna D, Kaye JA, Dodge HH, Erten-Lyons D, Rooney WD, et al. Characterizing the white matter hyperintensity penumbra with cerebral blood flow measures. NeuroImage Clin 2015; 8: 224–9.

Provenzano FA, Muraskin J, Tosto G, Narkhede A, Wasserman BT, Griffith EY, et al. White matter hyperintensities and cerebral amyloidosis: necessary and sufficient for clinical expression of Alzheimer's disease? JAMA Neurol 2013; 70: 455–61.

Roberts RO, Geda YE, Knopman DS, Cha RH, Pankratz VS, Boeve BF, et al. The mayo clinic study of aging: design and sampling, participation, baseline measures and sample characteristics. Neuroepidemiology 2008; 30: 58–69.

Schwarz AJ, Yu P, Miller BB, Shcherbinin S, Dickson J, Navitsky M, et al. Regional profiles of the candidate tau PET ligand 18F-AV-1451 recapitulate key features of Braak histopathological stages. Brain 2016; 139: 1539–50.

Schwarz CG, Gunter JL, Ward CP, Vemuri P, Senjem ML, Wiste HJ, et al. The mayo clinic adult life span template: better quantification across the life span. Alzheimers Dement 2017; 13: P792.

Senjem ML, Gunter JL, Shiung MM, Petersen RC, Jack CR. Comparison of different methodological implementations of voxel-based morphometry in neurodegenerative disease. NeuroImage 2005; 26: 600–8.

St Sauver JL, Grossardt BR, Yawn BP, Melton LJ III, Pankratz JJ, Brue SM, et al. Data resource profile: the Rochester epidemiology project (REP) medical records-linkage system. Int J Epidemiol 2012; 41: 1614–24.

St Sauver JL, Grossardt BR, Yawn BP, Melton LJ III, Rocca WA. Use of a medical records linkage system to enumerate a dynamic population over time: the Rochester epidemiology project. Am J Epidemiol 2011; 173(9): 1059–68.

Verhaaren BF, Vernooij MW, de Boer R, Hofman A, Niessen WJ, van der Lugt A, et al. High blood pressure and cerebral white matter lesion progression in the general population. Hypertension 2013; 61: 1354–9.